Lasing within live cells containing intracellular optical micro-resonators for barcode-type cell tagging and tracking

Marcel Schubert[1], Anja Steude[1], Philipp Liehm[1], Nils M. Kronenberg[1], Markus Karl[1],

Elaine C. Campbell[2], Simon J. Powis[2], and Malte C. Gather[1]*

[1] SUPA, School of Physics and Astronomy, University of St. Andrews, St Andrews, Fife, Scotland, United Kingdom

[2] School of Medicine, University of St. Andrews, St Andrews, Fife, Scotland, United Kingdom

ABSTRACT

We report on a laser that is fully embedded into a single live cell. By harnessing natural endocytosis of the cell we introduce a fluorescent whispering gallery mode (WGM) micro-resonator into the cell cytoplasm. On pumping with nanojoule light pulses, green laser emission is generated inside the cells. Our approach can be applied to different cell types and cells with micro-resonators remain viable for weeks under standard conditions. The characteristics of the lasing spectrum provide each cell with a barcode-type label which enables uniquely identifying and tracking of individual migrating cells. Self-sustained lasing from cells paves the way to new forms of cell tracking, intracellular sensing and adaptive imaging.

Integration of photonic and electronic devices into biological systems is a promising route to versatile biosensing and enhanced in-vivo imaging[1-6]. As sensing and imaging in biophotonics often relies on laser light, integration of lasers with biological systems is increasingly seen as a promising route to complementing and expanding the capability of current sensing and imaging techniques[7]. Like other lasers, such biointegrated laser sources will require three principal components—gain medium, optical feedback structure and pump source. Recently, naturally produced fluorescent proteins and vitamins were used as gain medium in different laser structures[8-10]. Cells expressing fluorescent protein were also utilized directly as gain medium[11,12]. However, these lasers required extracellular optical feedback structures that were much larger than typical cells and thus have limited potential for biointegration. Future applications of biolasers will require self-sustained generation of laser light, i.e. the integration of optical feedback into single cells without compromising their biological function.

Whispering gallery mode (WGM) micro-sphere resonators[13,14] confine light by total internal reflection and can provide optical feedback in a range of micro-laser configurations, e.g. as dielectric micro-spheres loaded with synthetic dyes[15,16]. Due to their large quality factor ($Q > 10^8$ has been reported)[13], compact size, and relative ease of fabrication, we hypothesize that they are promising for intracellular lasing when internalized by cells as schematically illustrated in Fig. 1a. The lasing wavelength and threshold of micro-sphere lasers depend critically on sphere size and on the refractive index contrast between the sphere and the surrounding medium. The micro-sphere resonators used in this work consisted of polystyrene divinylbenzene (PS-DVB) and had radii varying between 5 and 10 μm, i.e. smaller than most eukaryotic cells. Optical gain was provided by a green fluorescent dye ($\lambda_{em} = 510$ nm) doped into the micro-spheres. The

refractive index of PS-DVB at 510 nm is $n_{PS} = 1.60$, providing considerable index contrast for the micro-spheres to act as WGM resonators inside cells ($n_{cell} \approx 1.375$, Ref. [17]).

The ability of cells to internalize PS-DVB micro-spheres was tested with four different cell types: primary human macrophages, primary mouse microglia cells, mouse fibroblasts (NIH 3T3) and human embryonic kidney cells (HEK 293). A dispersion of PS-DVB micro-spheres was added to culture dishes containing the different cells and the interaction of the cells with the spheres was monitored under the microscope. Figure 1b and Supplementary Video 1 show a representative time-lapse series of a macrophage cell, starting 1 h after addition of the micro-spheres. During its random migration, the cell reached a micro-sphere (at time 14.8 min) and within less than five minutes internalized the entire sphere. Afterwards, the cell remained motile, dragging the internalized sphere along (time 18.2 to 26.7 min).

To study the internalization of micro-spheres further, we fluorescently labelled the nucleus and the cytoplasm of cells that were incubated with micro-spheres for 72 h and investigated them by confocal laser scanning microscopy (CLSM). Figure 1c shows a CLSM maximum intensity projection and a cross section for a typical macrophage (also see Supplementary Video 2). The high refractive index and the strong fluorescence of the micro-sphere distort the CLSM image, in particular the upper half of the sphere in the cross section. However, the images show clearly that the micro-sphere is fully enclosed by the cell. The same situation was observed for the other three investigated cell types (Figure 1d, Supplementary Figure 1). If kept at appropriate temperature and CO_2 level, cells containing micro-spheres remained viable for at least four weeks (the longest we studied so far).
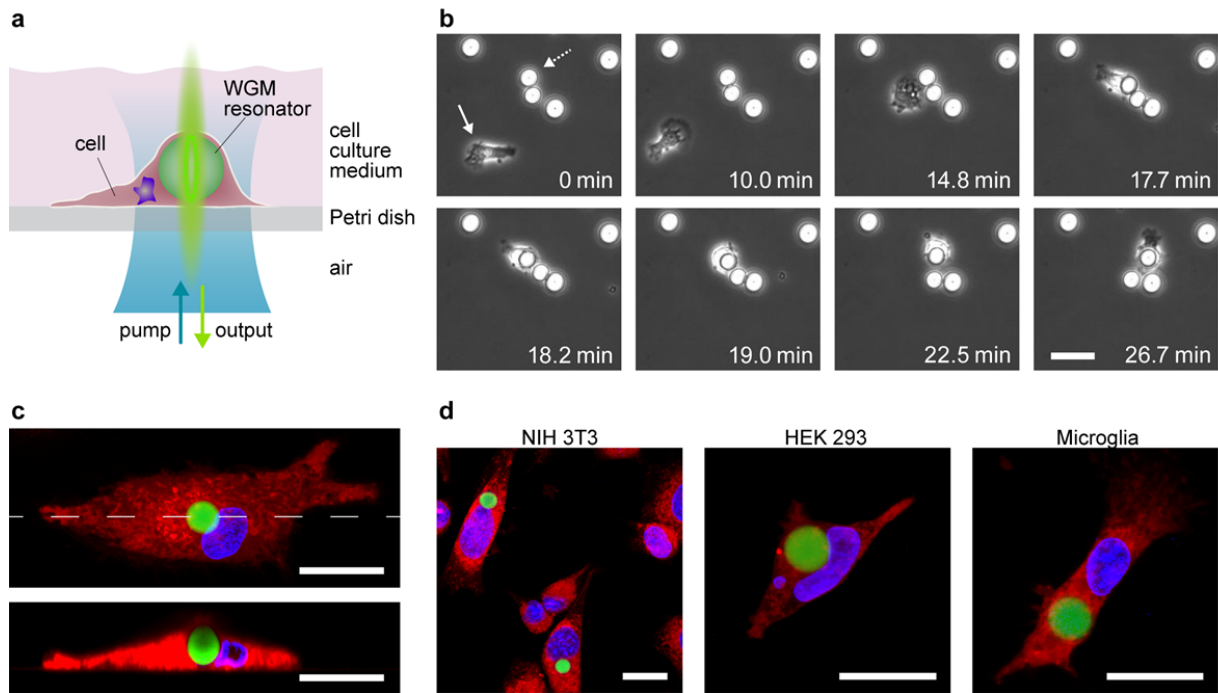
4

Figure 1. Self-sustained lasing from live cells containing intracellular optical resonators. (a) Schematic illustration of the intracellular laser. When kept under standard culture conditions cells internalize a whispering gallery mode micro-sphere resonator by natural endocytosis thereby eliminating the need for an extra-cellular resonator structure. Supply of pump light and detection of laser output are performed through a common imaging pathway. (b) Time-lapse microscopy of primary human macrophage cell (solid arrow) internalizing a micro-sphere resonator (dashed arrow). Numbers, time after start of measurement. (c) Confocal laser scanning microscopy (CLSM) data of a macrophage with cytoplasm (red fluorescence), cell nucleus (blue fluorescence) and internalized micro-sphere resonator (green fluorescence). Maximum intensity projection (top) and cross section along the dashed line (bottom). (d) Maximum intensity projection CLSM images for three further cell types—NIH 3T3 fibroblasts, Human Embryonic Kidney 293 and primary mouse microglia. For all three, spontaneous internalization of micro-sphere resonators is observed. Colours as in c. Scale bars in all panels, 20 μm.

Macrophages and microglia play an important role in the immune system and are capable of ingesting foreign objects (by endocytosis) that measure up to nearly twice their own diameter[18,19]. By contrast, NIH 3T3 and HEK 293 are cell lines without particularly pronounced capacity for endocytosis but these cells also readily internalized micro-spheres. Endocytosis of micrometre-sized objects has also been reported for other cell lines[20]. Introducing optical feedback structures in this way is thus a viable approach for a large variety of different cell types.

We next tested the ability of the micro-sphere containing cells to produce laser light. Using a custom-built microscope setup with 500 nm dichroic beam splitter, 40x objective and cell incubator, the nanosecond pulsed output of an optical parametric oscillator (OPO) laser system tuned to 470 nm was delivered to individual micro-sphere containing cells through the bottom of the culture dish. Emission from the cell was collected with the same objective, separated from back-reflected excitation light by the dichroic beam splitter and directed to a spectrometer.

Figure 2a shows the spectrally integrated emission of an individual cell as function of pump pulse energy. The data show a distinct threshold at 1.0 ± 0.1 nJ (corresponding to 0.6 mJ cm^{-2}); for higher pump energies, the increase in emission from the cell was significantly steeper than at low pump energies, strongly indicating lasing action within the cell.
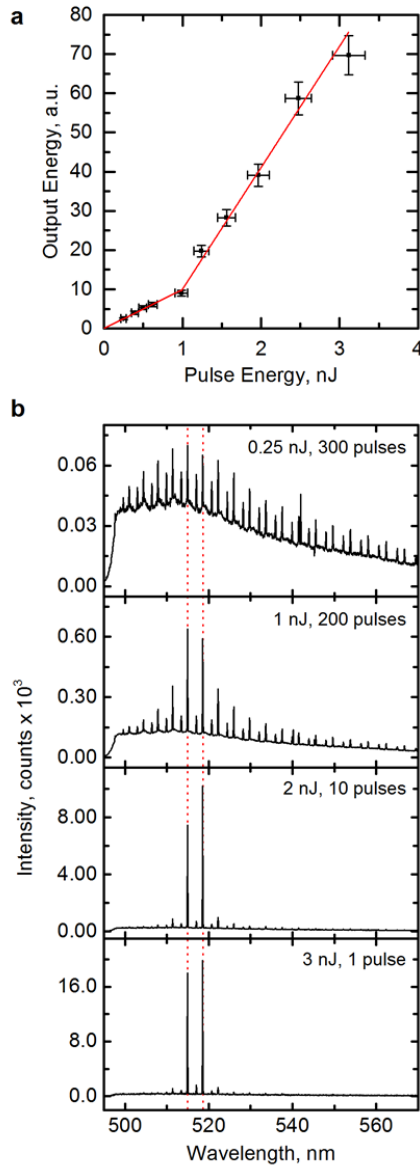
Figure 2. Characteristics of intracellular micro-sphere laser. (a) Output energy of laser as a function of energy of blue-light (470 nm) pump pulses. Red lines: linear fits to data below and above 1 nJ pump pulse energy. (b) Output spectra below threshold (0.25 nJ), at threshold (1 nJ) and at two points above the lasing threshold (2 and 3 nJ). Dotted red lines mark the two wavelengths of laser emission. Pulse number indicates number of pump pulses required to acquire the respective spectrum.

For pump energies below the lasing threshold, the emission spectrum of the micro-sphere showed a series of regularly separated pairs of emission peaks; each larger peak was paired with a weaker blue-shifted peak (Fig. 2b, 0.25 nJ). This pattern is consistent with coupling to the transverse electric (TE, larger peaks) and transverse magnetic (TM, smaller blue-shifted peaks) modes of the WGM resonator[13,14]. (TE and TM are defined with respect to the micro-sphere surface, Supplementary Fig. 2.) Around the lasing threshold, two TE peaks close to the maximum emission wavelength of the green fluorescent dye began to gain in relative intensity (1 nJ) and eventually completely dominated the emission spectrum (2 and 3 nJ), providing further evidence for laser action inside the cell. (Lasing is expected to occur predominantly from TE modes due to their higher quality factor[16].) Over the investigated range of pump energies, the spectral position of the peaks shifted by < 0.05 nm. We note that above the lasing threshold a clean spectrum can be obtained by collecting light from just one laser pulse, while below threshold integration over hundreds of pulses was necessary to achieve good signal-to-noise ratio.

To confirm that the observed spectral pattern is due to a series of TE and TM modes of the WGM resonator (with different angular mode numbers l), we calculated the wavelengths of these modes by solving the 2D polar Helmholtz equation[21]. Assuming $n_{PS} = 1.6$ and $n_{cell} = 1.375$, the peaks at 514.9 nm and 518.6 nm correspond to TE modes with $l = 135$ and 134, respectively, and to a micro-sphere radius of 7.41 μm, consistent with microscope images of the investigated cell.

The dominant lasing wavelength (λ_{max}) and the spacing between the two TE peaks in the lasing spectrum ($\Delta\lambda$) differ between different intracellular lasers. We propose to use this as barcode-type cell label to unambiguously distinguish a large number of cells and to track cell migration over an extended period of time. To illustrate this concept, the migration of a group of

macrophages with internalized micro-spheres was followed for 19 h (Figure 3a, Supplementary Video 3). All cells were motile and changed shape over the course of the experiment, but migration patterns varied between cells as expected. The lasing spectrum of each cell was recorded at 0, 7 and 19 h (Figure 3b). Each cell was characterized by a unique spectrum that was clearly different from the spectra of all other cells and that remained unchanged over the entire course of the experiment, indicating that the spectrum is specific to each intracellular laser and showing clearly that the resonator is not damaged during the experiment. Only for one cell (Cell C3), λ_{max} shifted by a noticeable amount (between 7 h and 19 h). However, even here the shift was only 0.15 nm and $\Delta\lambda$ was not affected ($\Delta\lambda = 4.638$ nm).

The cells remained viable and highly motile over the entire 19 h course of the measurement (during which the lasing spectra were recorded three times) and cells transported the micro-sphere resonators over substantial distances (many times the size of the cells). Cell damage was only observed when we pumped the cells continuously for several minutes, i.e. by several thousand pump pulses, and well above the threshold. Such extreme conditions are not required for any foreseeable application of the cell lasers as the complete spectrum can be obtained by a single excitation pulse. The light dose a cell is exposed to when acquiring its lasing spectrum (pump flux, ~1 mJ cm^{-2}) in fact is equivalent to the dose needed to record a typical epi-fluorescence image (100 ms exposure at 10 mW cm^{-2}). We further found that the viability of macrophages over a 3 week time-course (the longest we studied so far) was the same for cells with and without internalized micro-spheres, indicating that the resonators are not harmful to the cells.
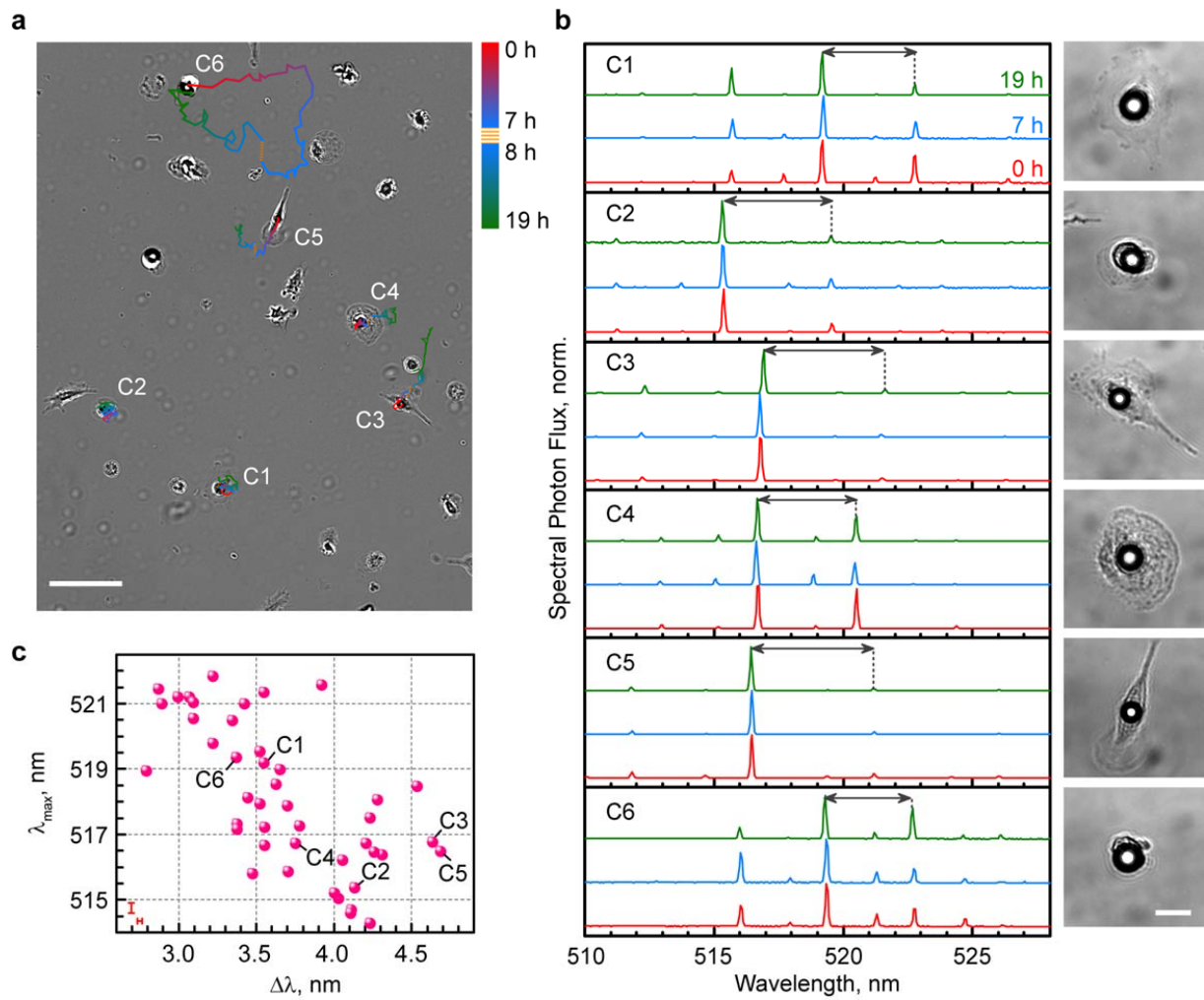
Figure 3. Application of emission from intracellular lasers as tags for tracking and identification of individual freely migrating cells. (a) Bright-field image of six primary macrophage cells with internalized micro-sphere resonators (labelled C1 to C6) at the beginning of the experiment. Coloured solid traces indicate the migration path of each cell over the 19 h time frame of the experiment. Orange dashed lines indicate time gap during which lasing experiments were performed. Scale bar, 100 μm. (b) Left: Lasing spectra from each cell at 0 h, 7 h and 19 h. Arrows indicate spectral separation between the transverse electric (TE) modes (Δλ). Right: Bright field images of each cell at 0h. Scale bar, 20 μm. (c) Dominant lasing wavelength (λ_max) and Δλ provide a unique tag for individual intracellular lasers. λ_max and Δλ for a population of

randomly selected intracellular lasers from the same dish as in b. Cells from b are labelled. Error bars, TE mode separation ±0.015 nm (resolution of spectrometer), λ_{max} ±0.15 nm (derived from wavelength shift of Cell C3 in b).

Figure 3c summarizes λ_{max} and $\Delta\lambda$ for the cells from Figure 3b and for a further 35 cells (brightfield images, Supplementary Figure 3) from the same culture dish and shows that all but two cells can be reliably distinguished. (All intracellular lasers had thresholds of 0.5 - 7 nJ.) For the micro-spheres used here, λ_{max} was within a range of 8 nm, and $\Delta\lambda$ varied by 2 nm. Given the temporal stability of λ_{max} and $\Delta\lambda$ and the small uncertainty in measuring them (0.3 nm for λ_{max} and 0.03 nm for $\Delta\lambda$; see error bars in Figure 3c), one could track over a thousand cells without overfilling the λ_{max}-$\Delta\lambda$ parameter space. Assuming that intracellular lasers are distinguishable if the spectral separation is at least twice the measurement uncertainty, the number of distinguishable lasers is (8 nm/0.3 nm) × (2 nm/0.03 nm) ≈ 1800. On the $\Delta\lambda$ axis the 0.03 nm uncertainty corresponds to an ability to distinguish resonators that differ in radius by 35 nm. In the future, even smaller size difference could be resolved by using a higher resolution spectrometer. In this context the narrow linewidth of intracellular lasers is advantageous over non-lasing micro-sphere resonators, analogous to the situation for WGM biosensors[16].

In the future, to increase the number of uniquely tagged cells further, micro-spheres stained with different dyes can be spectrally multiplexed. In our experiments, cell lasing occurs across an approximately 10 nm spectral range close to the emission peak of the dye, therefore enabling use of a larger number of dyes than would be possible with conventional fluorescence spectroscopy where multiplexing is usually limited to four to five dyes across the visible part of the spectrum (400 to 700 nm). Based on the 10 nm spectral range, we estimate that about 30 different dyes

11

emitting across the visible spectrum could be used for staining micro-spheres, yielding a total of ~10^5 cells that can be unambiguously tagged.

Our method can be applied in scenarios where tracking cells from a sequence of bright-field images is impossible or impractical, e.g. for long-term studies involving multiple dishes that cannot be monitored continuously, for confluent cells, for cells in 3D tissue scaffolds and to tag cells *in vivo*. Read-out of the lasing characteristics requires only one ns pump pulse (see Fig. 2b, 3 nJ), rendering our approach well suited for high throughput detection. Existing cell tagging techniques rely on spectrally distinct fluorescent dye or quantum dot tags, on imaging barcode-type microstructures attached to cells[22,23] or on microscopic radio-frequency (RF) identification tags[24]. Our intracellular laser tags offer several unique advantages over these: They facilitate tracking of a vastly larger number of different cells than fluorescent tags; their fabrication is less complex than for RF and microstructure tags; they can be localized with better spatial resolution than RF tags; the requirements for optical access are less stringent than for imaging microstructures which is particularly relevant for applications in tissue scaffolds or *in vivo*.

From the width of the emission peaks in the sub-threshold emission spectrum of one of the smallest intracellular lasers that we analyzed (radius 6.5µm, threshold 5 nJ), we estimate that the quality factor of this resonator is $Q \approx 10,000$. From this number, the modal optical gain at threshold can be estimated as $g_{th} = \frac{2\pi n}{Q\lambda_0} \approx 19$ cm^{-1}, consistent with the gain available in state-of-the-art organic gain materials[25] (modal refractive index $n \approx n_{PS}$; λ_0, vacuum wavelength). In the future, shrinking resonator size is likely to simplify integration with cells further. To evaluate routes to reducing resonator size, we estimated the dependence of the quality factor Q of a micro-sphere resonator located inside a cell (n_{cell} = 1.375) on sphere radius and refractive index, using again the polar Helmholtz equation approach (Figure 4). With increasing radius, Q initially

grows quickly but then reaches an upper limit given by material absorption. The absolute value of Q depends strongly on the refractive index of the micro-sphere. While the widely used low-index fused silica ($n = 1.46$) micro-spheres do not achieve useful Q at biologically relevant radii when inside a cell, barium titanate micro-spheres (BaTiO$_3$, $n = 2.14$) reach $Q \approx 10{,}000$ at a 3.8 times smaller radius than PS-DVB micro-spheres (see inset of Figure 4), reducing the volume of the resonator by a factor of 55. Finally, other resonator concepts, in particular metal based plasmonic cavity structures, may provide further scope for reducing resonator size[26,27].
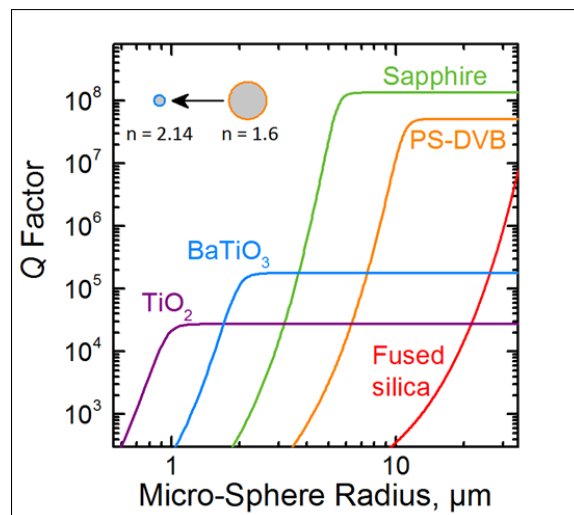

Figure 4. Calculated Q factors for WGM micro-sphere resonators made of different optical materials as a function of resonator size. The surrounding medium was assumed to have a refractive index of 1.375 (the average refractive index of a typical cell). For PS-DVB and quartz, a vacuum wavelength of $\lambda_0 = 520$ nm was assumed; data for the other materials was computed at $\lambda_0 = 600$ nm where the absorption of these materials is less. The inset illustrates the relative sizes of a PS-DVB and a BaTiO$_3$ micro-sphere, with 5.7 μm and 1.5 μm radius, respectively; both micro-spheres have a predicted Q factor of 10,000. Numbers indicate the refractive index of each material.

In contrast to previous demonstrations of biolasing, the intracellular WGM lasers presented here are fully contained within single cells, are formed by a natural, biologically driven process that can be readily scaled[28], and enable unique tagging and tracking of large numbers of cells. We expect that this breakthrough in biointegration of micro-lasers will lead to applications in structural and functional *in vivo* imaging: Intracellular lasers pumped by non-ballistic diffuse photons may be used to monitor the migration of macrophages to sites of inflammation[29] and dendritic cells in local lymph nodes[30], thus visualizing local structures during immune responses or to map the trajectory of circulating tumor cells[31].

Methods

Cell culture and micro-sphere internalization: Plastic adherent CD14$^+$ macrophage cells were isolated from blood samples obtained from normal healthy human donors under informed ethical consent from the School of Medicine, University of St Andrews. Flow cytometry confirmed the cells as CD14+ macrophages (Supplementary Fig 4). Microglia cells were isolated from the cerebral cortex of postnatal day 2 mice following the procedure described in Ref. [32]. NIH 3T3 and HEK 293 cells were obtained from Sigma Aldrich. Cells were cultured in RPMI (primary macrophages) or DMEM (microglia, HEK 293, NIH 3T3) medium with 10vol% fetal calf serum and 1vol% penicillin-streptomycin solution. 10vol% horse serum were added for microglia cultures. PS-DVB micro-spheres that were internally stained with the Firefli™ Green dye were purchased from Fisher Scientific. Staining was stable in water and ethanol. Micro-spheres were dispersed in 70% ethanol and incubated for 1h for sterilization. Ethanol was exchanged for PBS buffer and the micro-sphere concentration was adjusted to 2×10^6 mL^{-1}. 10 µL of the dispersion were added to a dish containing 2 mL of culture medium and the previously prepared cells.

Imaging of resonator uptake: To observe uptake of the micro-sphere resonators, the cell containing dishes were transferred to a stage-top microscope incubator (OkoLab, H301, set to 37°C, 5% CO_2, 95% rel. humidity) and observed with an inverted optical fluorescence microscope (Nikon, Ti-S). Long-term cell viability was assessed by observing cell motility and proliferation. CLSM (Leica, TCS SP8) was used to image the cell cytoplasm (red fluorescence, stained with CellTracker[TM] dye, LifeTechnologies), the cell nucleus (blue fluorescence, Hoechst 33342, Sigma Aldrich) and the internalized micro-sphere resonator (green fluorescence). Cells were stained 1 to 2 h prior to CLSM and transferred to pH indicator-free medium right before the measurements to reduce background fluorescence. CLSM was performed under standard ambient conditions.

Laser characterization: A custom built microscopy setup was used for laser characterization. The cell containing dish was transferred to a stage-top microscope incubator mounted on a micro-positioning stage. Koehler type bright-field illumination with a white LED and a 10x or 40x objective were used to image cells. Optical pumping was achieved by an OPO laser system (Opotek; pulse duration, 5 ns; set to 10 Hz repetition rate). Pump light was directed onto individual cells with a dichroic mirror (500 nm, long-pass) and the 40x objective, yielding a pump-spot diameter of ~15 µm. Emission from the cells was collected through the same objective, passed through the dichroic mirror and a further 500 nm long-pass filter and imaged onto the entrance slit of a 500 mm spectrograph coupled to a cooled CCD camera (Andor). To determine the Q-factor of the micro-spheres, lasing spectra were recorded with a high resolution grating (1800 lines mm^{-1}) and Q was computed as the ratio of peak wavelength over peak width ($\lambda/\Delta\lambda$). Neutral density filters were used to adjust the energy of the pump pulses. Pump pulse energy was monitored with an energy meter. Pulse energies quoted here are for a single pulse

and measured behind the 40x objective, i.e. they correspond directly to the pulse energy incident on the cell and the resonator. The output energy of the intracellular laser was determined by integrating the emission spectra between 514 and 520 nm.

Cell tagging and tracking: For the cell tracking experiments a series of overview images were recorded with a 10x objective. The migration path of each cell was extracted using the Fiji software with the plugin MTrackJ[33]. Lasing characteristics were recorded with a 40 x objective for each cell at defined time points as described above.

ASSOCIATED CONTENT

Supporting Information

Additional CLSM data, hyperspectral images, bright field images of the intracellular lasers from Figure 3c, flow cytometry data, time lapse video of bead uptake, CLSM z-stack video and time lapse video of cell tagging experiment. This material is available free of charge via the Internet at http://pubs.acs.org.

AUTHOR INFORMATION

Corresponding Author

*Email address: mcg6@st-andrews.ac.uk

Author Contributions

MS characterized intracellular lasers, designed the cell tracking experiment, and performed and analysed CLSM measurements. AS carried out cell culturing and staining, and assisted in

preparing CLSM measurements. AS and NMK recorded time lapse microscopy data and analysed bead uptake. PL prepared microglia cells. ECC and SJP prepared and analysed macrophage samples. MK and MCG performed optical simulations. MCG conceived and supervised the project, designed the intracellular lasing experiments and wrote the manuscript with input and discussion from all authors. All authors have approved the final version of the manuscript.

Notes

The authors declare no competing financial interest.

REFERENCES

1	Kim, T. I. *et al.* Injectable, Cellular-Scale Optoelectronics with Applications for Wireless Optogenetics. *Science* **340**, 211-216 (2013).

2	Yan, R. X. *et al.* Nanowire-based single-cell endoscopy. *Nat. Nanotechnol.* **7**, 191-196 (2012).

3	Shambat, G. *et al.* Single-Cell Photonic Nanocavity Probes. *Nano Lett.* **13**, 4999-5005 (2013).

4	Omenetto, F. G. & Kaplan, D. L. New Opportunities for an Ancient Material. *Science* **329**, 528-531 (2010).

5	Hwang, S. W. *et al.* A Physically Transient Form of Silicon Electronics. *Science* **337**, 1640-1644 (2012).

6	Ghezzi, D. *et al.* A polymer optoelectronic interface restores light sensitivity in blind rat retinas. *Nat. Photonics* **7**, 400-406 (2013).

7	Fan, X. & Yun, S.-H. The potential of optofluidic biolasers. *Nature Methods* **11**, 141-147 (2014).

8	Vannahme, C., Maier-Flaig, F., Lemmer, U. & Kristensen, A. Single-mode biological distributed feedback laser. *Lab Chip* **13**, 2675-2678 (2013).

9	Chen, Q. S. *et al.* Highly sensitive fluorescent protein FRET detection using optofluidic lasers. *Lab Chip* **13**, 2679-2681 (2013).

10	Nizamoglu, S., Gather, M. C. & Yun, S. H. All-Biomaterial Laser Using Vitamin and Biopolymers. *Adv. Mater.* **25**, 5943-5947 (2013).

11	Gather, M. C. & Yun, S. H. Single-cell biological lasers. *Nat. Photonics* **5**, 406-410 (2011).

12	Jonáš, A. *et al.* In vitro and in vivo biolasing of fluorescent proteins suspended in liquid microdroplet cavities. *Lab Chip* **14**, 3093-3100 (2014).

13	Chiasera, A. *et al.* Spherical whispering-gallery-mode microresonators. *Laser Photon. Rev.* **4**, 457-482 (2010).

14	Vollmer, F. & Yang, L. Label-free detection with high-Q microcavities: a review of biosensing mechanisms for integrated devices. *Nanophotonics* **1**, 267-291 (2012).

15	Kuwata-Gonokami, M. & Takeda, K. Polymer whispering gallery mode lasers. *Opt. Mater.* **9**, 12-17 (1998).

16	Francois, A. & Himmelhaus, M. Whispering gallery mode biosensor operated in the stimulated emission regime. *Appl. Phys. Lett.* **94**, 031101 (2009).

17	Ekpenyong, A. E. *et al.* Bacterial infection of macrophages induces decrease in refractive index. *J. Biophotonics* **6**, 393-397 (2013).

18	Murray, P. J. & Wynn, T. A. Protective and pathogenic functions of macrophage subsets. *Nat. Rev. Immunol.* **11**, 723-737 (2011).

19	Cannon, G. J. & Swanson, J. A. The macrophage capacity for phagocytosis. *J. Cell Sci.* **101**, 907-913 (1992).

20	Gratton, S. E. A. *et al.* The effect of particle design on cellular internalization pathways. *Proc. Natl. Acad. Sci. U. S. A.* **105**, 11613-11618 (2008).

21	Bohren, C. F. & Huffman, D. R. *Absorption and scattering of light by small particles.* (John Wiley & Sons, 2008).

22	Fernandez-Rosas, E. *et al.* Intracellular polysilicon barcodes for cell tracking. *Small* **5**, 2433-2439 (2009).

23   Novo, S. *et al.* A novel embryo identification system by direct tagging of mouse embryos using silicon-based barcodes. *Human Reproduction* **26**, 96-105 (2011).

24   Chen, L. Y. *et al.* Mass fabrication and delivery of 3D multilayer µTags into living cells. *Scientific Reports* **3**, 2295 (2013).

25   Samuel, I. D. W. & Turnbull, G. A. Organic semiconductor lasers. *Chem. Rev.* **107**, 1272-1295 (2007).

26   Hess, O. *et al.* Active nanoplasmonic metamaterials. *Nat. Mater.* **11**, 573-584 (2012).

27   Ma, R. M., Oulton, R. F., Sorger, V. J. & Zhang, X. Plasmon lasers: coherent light source at molecular scales. *Laser Photon. Rev.* **7**, 1-21 (2013).

28   Wu, Y.-C. *et al.* Massively parallel delivery of large cargo into mammalian cells with light pulses. *Nature Methods* **12**, 439-444 (2015).

29   Grabher, C. *et al.* Birth and life of tissue macrophages and their migration in embryogenesis and inflammation in medaka. *J. Leukoc. Biol.* **81**, 263-271 (2007).

30   Stoll, S., Delon, J., Brotz, T. M. & Germain, R. N. Dynamic imaging of T cell-dendritic cell interactions in lymph nodes. *Science* **296**, 1873-1876 (2002).

31   Zhe, X. N., Cher, M. L. & Bonfil, R. D. Circulating tumor cells: finding the needle in the haystack. *Am. J. Cancer Res.* **1**, 740-751 (2011).

32   Mecha, M. *et al.* An easy and fast way to obtain a high number of glial cells from rat cerebral tissue: A beginners approach. *Protocol Exchange* (2011).

33   Meijering, E., Dzyubachyk, O. & Smal, I. Methods for Cell and Particle Tracking *Methods in Enzymology* **504**, 183-200 (2012).

Table of Contents Graphic